SAN096-1424C
96306
CONF-960805--2

SOLAR HEAT PIPE TESTING OF THE STIRLING THERMAL MOTORS 4-120 STIRLING ENGINE

Charles E. Andraka, K. Scott Rawlinson, Timothy A. Moss, Douglas R. Adkins,
James B. Moreno, Donald R. Gallup, Patricia G. Cordeiro
Sandia National Laboratories
Albuquerque NM 87185

Stefan Johansson
Stirling Thermal Motors, Inc.
275 Metty Drive
Ann Arbor, MI 48103

ABSTRACT

Stirling-cycle engines have been identified as a promising technology for the conversion of concentrated solar energy into usable electrical power. A 25kW electric system takes advantage of existing Stirling-cycle engines and existing parabolic concentrator designs. In previous work, the concentrated sunlight impinged directly on the heater head tubes of the Stirling Thermal Motors (STM) 4-120 engine.

A Sandia-designed felt-metal-wick heat pipe receiver was fitted to the STM 4-120 engine for on-sun testing on Sandia's Test Bed Solar Concentrator. The heat pipe uses sodium metal as an intermediate two-phase heat transfer fluid. The receiver replaces the directly-illuminated heater head previously tested. The heat pipe receiver provides heat isothermally to the engine, and the heater head tube length is reduced, both resulting in improved engine performance. The receiver also has less thermal losses than the tube receiver. The heat pipe receiver design is based on Sandia's second-generation felt-wick heat pipe receiver.

This paper presents the interface design, and compares the heat pipe/engine test results to those of the directly-illuminated receiver/engine package.

INTRODUCTION

Dish-Stirling systems have demonstrated the potential to produce economical environmentally-acceptable electric power from the sun. In 1984, the Advanco-Vanguard dish-Stirling module demonstrated a world record peak net conversion efficiency of sunlight to electricity of 29.4% (Washom, 1984). McDonnell Douglas Corp. further developed a system based on the Advanco module (Coleman and Raetz, 1986). Recently, dish-Stirling system development by the Department of Energy (DOE) through Sandia National Laboratories, the National Renewable Energy Laboratory, and industry has shifted from component research and development to an emphasis on commercialization of dish-Stirling systems. Science Applications International Corporation (SAIC) is developing such a system with Stirling Thermal Motors (STM). The system incorporates STM's 4-120 Stirling engine and the SAIC faceted stretched-membrane dish (Figure 1). The system is nominally designed to produce 25kW$_e$ of grid-quality electricity.

The SAIC system uses convoluted heater-head tubes on the four-cylinder engine, shaped to directly absorb the concentrated solar flux. During initial testing, the performance of the engine has been limited by the peak temperatures measured and predicted on the heater head tubes. SAIC has re-aligned the dish slightly, reducing the peak incident fluxes at the expense of a larger receiver aperture and therefore greater thermal losses. The system is currently operating in this mode, producing a peak power of 21.4kW$_e$ to the grid. STM has made significant

FIGURE 1. SAIC FACETED STRETCHED-MEMBRANE DISH WITH THE STM 4-120 ENGINE OPERATING ON SUN.

improvements to the engine to increase life, reduce cost, and increase the power potential. SAIC is re-designing the concentrator to provide additional thermal power to the engine. However, this approach will likely proportionally increase the thermal peak flux, and therefore the peak heater head temperature, which is limited by materials considerations. Thus, an alternate receiver approach may be needed.

The reflux receiver was conceived as an improvement over directly illuminated tube receivers (Diver et al, 1990). In the reflux receiver, liquid metal (sodium and/or potassium) is evaporated at the solar absorber and condensed at the engine heater tubes, supplying the latent heat of vaporization to the engine. The liquid at the absorber may be a pool that floods the surface (pool boiler) or a wick saturated with liquid metal that covers the absorber surface (heat pipe). The condensate is returned to and distributed over the absorber by gravity (refluxing), wick capillary forces, or a combination thereof. The reflux receiver has the important advantage of nearly-isothermal operation even with non-uniform incident solar-flux distributions. In addition, the reflux receiver permits relatively-independent design and optimization of the absorber (receiver) and the engine heater tubes. The phase-change of the working fluid potentially provides significant tolerance to high peak thermal fluxes.

Over the last two years, Sandia has identified and tested a promising heat-pipe wick structure using sintered metal fibers (Andraka et al, 1995). The wick has the potential to double the throughput performance of more conventional heat-pipe wick structures. Recent on-sun and bench-scale testing has demonstrated the potential of this technology to meet the needs of the SAIC/STM system. The current work provides the unique opportunity to test both a Directly-Illuminated Receiver (DIR) and a heat-pipe receiver on the same engine and concentrator, allowing an evaluation of the system performance changes attributed to the reflux receiver technology. In addition, we also operated the DIR version with hydrogen as the working fluid, replacing the previous helium. The hydrogen provides some system performance improvements without adding complexity to the receiver. However, permeation of the hydrogen through the heater head walls into the heat pipe prevent its use on the heat pipe system at this time.

SYSTEM DESCRIPTION

The STM Power Conversion System (PCS) consists of an engine, receiver, cooling system, control system, and the enclosure/mounting structure (Figure 2).

STM's STM4-120 engine is a four cylinder, double acting Stirling engine. The swept volume of each cycle is 120-cc. The working fluid is helium with a nominal mean operating pressure of 13MPa. The cycle temperature at the hot end is approximately 700 °C, while typical cooling water temperatures are about 40 °C. In contrast to pressure control engines, STM's engine uses a hydraulically-actuated variable swashplate to control piston stroke, and therefore engine power. To reduce the differential pressure across the piston rod seals, STM uses a pressurized crankcase charged to about 6MPa. The engine is rated for a power output of 25kWe, and the engine shaft efficiency is rated at approximately 40% depending on operating conditions.

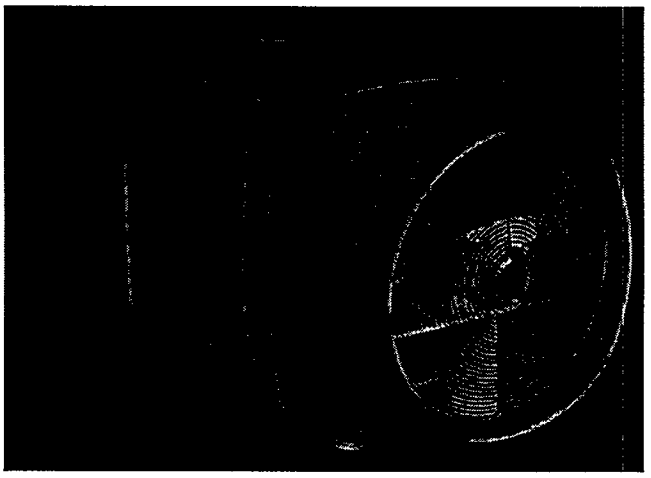

FIGURE 2. STM POWER CONVERSION SYSTEM (PCS), SHOWING THE COOLING FAN AND RADIATOR.

The heat is input to the engine through four heater heads, one for each cylinder. In the first tests, the tubes of the heater head are directly illuminated by the concentrated solar flux. In the most recent tests, an intermediate heat transfer fluid (sodium) is vaporized by the solar flux and condenses on the heater head tubes. Heat rejection is accomplished by circulating a water/glycol mixture through the engine coolers. The cooler is essentially a tube-and-shell heat exchanger, with helium flowing inside the tubes, and water/glycol flowing around the tubes. Heat is rejected to the atmosphere using three high-efficiency radiators mounted around the perimeter of the package.

The control system for the engine is also part of the PCS. The controller monitors all of the temperature, pressure, and level sensors and issues a shutdown signal if any parameter is out-of-range. The control input signal is the highest-reading receiver thermocouple. The control output is a signal to control the swashplate angle via a spool valve, which hydraulically moves the swashplate actuator.

All of these components are mounted in one package. All components are attached to an internal steel structure which interfaces to the concentrator. A fiberglass shell encloses all of the components (except for the radiators) and protects them from the elements.

The PCS was tested on the Test Bed Concentrator (TBC) at the National Solar Thermal Test Facility (NSTTF). The TBC is a modified antenna structure, with elevation-over-azimuth tracking. There are 220 glass mirrors mounted on parabolic shaped framework. Each mirror has a spherical contour. Peak concentration at the focal point is about 1500 W/cm^2 while concentrations on the receiver surface range from 0-70 W/cm^2 at 1000 W/m^2 insolation. Thermal power is in the 75-80 kW range. Input power can be reduced by applying mirror covers to any number of facets.

The PCS is mounted to a ring structure located behind the focal point of the concentrator (Figure 4). Instrumentation and control lines run from the ring to the control room. Data is collected using an HP3852 scanner/voltmeter controlled by a PC with LabView data acquisition software. A solar-blind infrared

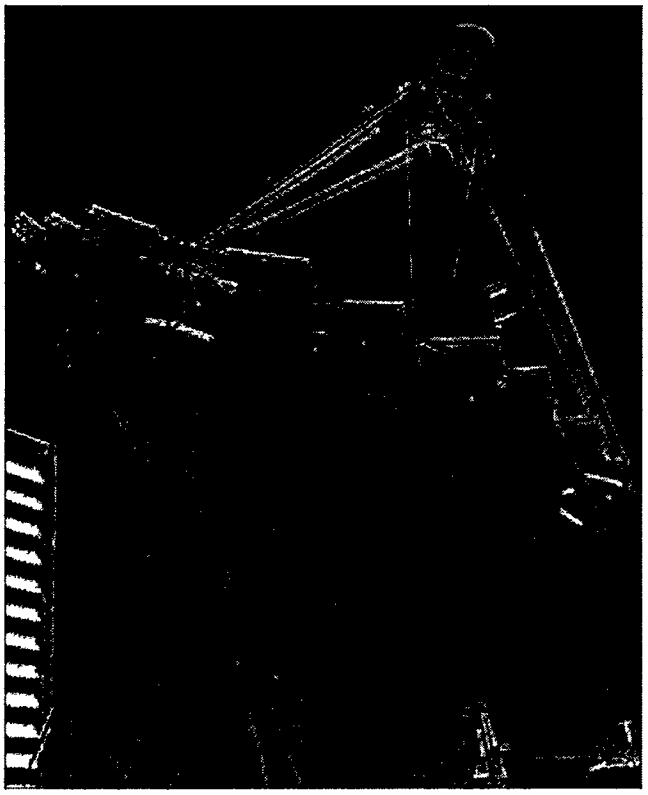

FIGURE 4. STM PCS AS TESTED ON SANDIA'S TEST BED CONCENTRATOR.

camera is used to monitor the temperature of the illuminated surface of the receiver.

DIRECTLY-ILLUMINATED RECEIVERS

Design

For the first set of tests, heat input to the engine was supplied by a direct-illumination receiver. There are four individual quadrants of heater tubes, one for each cycle. Each head consists of a regenerator housing, eighteen heater tubes, and the cylinder housing. The housings are made from XF-818, while the heater tubes are made from Inconel 625. When all four quadrants are mounted on the engine block, the assemblies form a circular receiver 400 mm in diameter, with all the tubes in a slight swirl pattern (Figure 3). With this arrangement, the heater tubes are directly exposed to the incident flux, heating the helium flowing inside the tubes.

A ceramic plug protects the center of the engine from any incident flux. The flux in this center area is less than 10W/cm^2 because of blockage from the PCS. This plug is shaped to re-radiate energy to the heater tubes. The heater heads are wrapped with Kaowool blanket insulation, while a conical aperture is made from FiberFrax rigid insulation. To limit the convective and radiation heat losses, the aperture boards were tapered from the outer edge of the receiver to 220-mm at the focal plane of the concentrator.

Receiver tube absorptance is dependent on the amount of surface oxidation. In order to provide a uniformly high absorptance (about 85%), STM pre-oxidizes the tubes in an air furnace oven. The receiver tube length was determined by the conflicting requirements of short tubes for high engine performance and long tubes for low peak solar fluxes. The increased tube length required results in an increase in the engine dead volume, which results in a slight performance penalty.

Test Results

The STM engine package was tested with both helium and hydrogen as the engine working fluid. Helium has the advantage of being an inert gas. Hydrogen is more conductive and has a lower viscosity and therefore lower flow losses than helium. However, hydrogen is more hazardous, is more difficult to contain, and possibly causes hydrogen embrittlement. STM plans to use chosen to use hydrogen in their first generation commercial systems to take advantage of the improved performance.

During the first series of tests, we used helium as the working fluid and covered 28 mirror facets to control peak receiver fluxes. The receiver was controlled at 750°C, 775°C, and 800°C. At these temperatures net PCS efficiency (nets out PCS fan/pump/controller parasitics) ranged from 23.2% to 25.2%, while net system efficiency ranged from 20.5% to 22.2%. Gross PCS efficiency ranged from 24.4% to 26.4%, while gross system efficiency ranged from 21.6% to 23.5%. Measured gross power output ranged from 16.6kW$_e$ to 17.8kW$_e$.

In the next series of tests, we used hydrogen as the working fluid under the same control conditions. The net PCS efficiency ranged from 25.7% to 27.1%, while net system efficiency ranged from 23.2% to 24.5%. Gross PCS efficiency ranged from 27.1% to 28.4%, and gross system efficiency ranged from 24.5% to

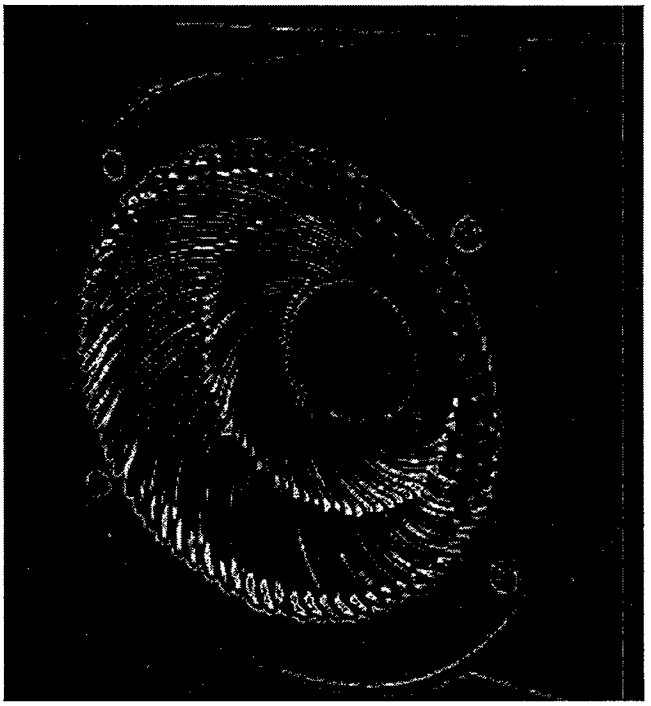

FIGURE 3. STM DIR RECEIVER HEATER HEAD TUBES, WITH THE CONICAL APERTURE REMOVED FOR CLARITY.

25.7%. Measured gross power output ranged from 17.6 kW_e to 19.5 kW_e.

Comparing the two tests, hydrogen increases the PCS and system efficiencies by about 2% points, and power output increases by about 1.5kW_e under similar operating conditions.

The above tests were not performed at full dish power, but with 28 mirror facets covered. This is because the peak receiver temperatures exceeded the design limits at higher input power levels. The receiver control temperature is based on the highest of the 28 thermocouples brazed to the back side of the receiver tubes. Four additional thermocouples were brazed to the front surface of the receiver tubes to indicate the ΔT between the front and back tube surface and to provide a reference for the IR camera. We measured ΔT's of approximately 100 °C, which agrees well with a previous STM estimate and our own finite element analysis results.

HEAT PIPE RECEIVER

Design

The heat-pipe receiver utilizes a stainless steel felt wick developed by Sandia and Porous Metal Products (Andraka et al, 1995 and Adkins et al, 1995). A second-generation receiver is used, which consists of a 416mm diameter absorber dome with a half-sphere angle of 70°, supported by a full hemisphere rear dome (Figure 5). The wick consists of two layers of 4-micron-fiber felt, sintered to the Haynes-230 allow dome. Four 51mm-diameter vapor ducts deliver the sodium vapor to the four heater heads (Figure 6), and the condensate is returned to the absorber via 9.5mm-diameter liquid return lines located inside the vapor ducts. The liquid is returned directly to the wick structure rather than to the pool. The receiver is mounted to the engine with two vertical and one horizontal a-frame strut assemblies which allow for the thermal expansion of the receiver. The locations and angles of the vapor tubes are such that the differential thermal expansion of the receiver, engine block, and support brackets results in axial compression of the vapor tubes. This compression is absorbed by Inconel 600 bellows in each vapor line. The receiver is charged with 1300g of sodium, using a reflux filling

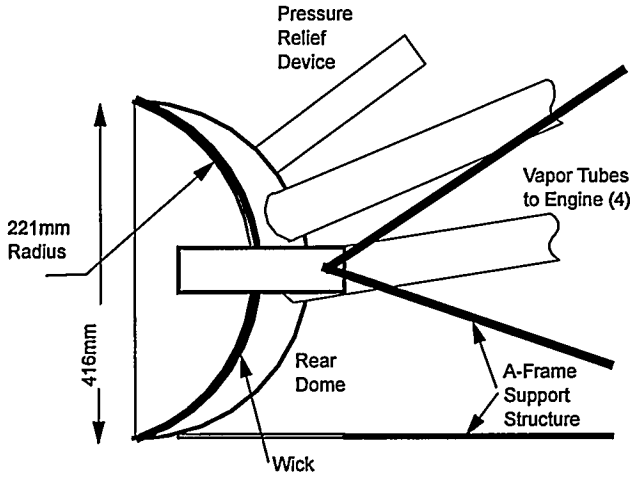

FIGURE 5. SCHEMATIC OF THE SECOND-GENERATION HEAT-PIPE RECEIVER.

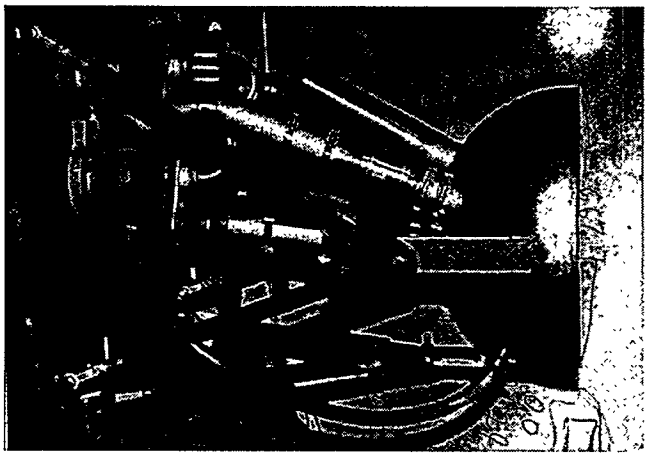

FIGURE 6. HEAT PIPE RECEIVER SHOWING VAPOR DUCT ARRANGEMENT TO HEATER HEADS.

operation intended to reduce and remove the oxide layer from the capillary wick structure (Adkins, 1996).

The receiver was fitted with white ceramic insulation sidewalls, tapering down to an 220mm-diameter aperture to limit re-radiation losses. The rim of the receiver was located 100mm behind the focal point of the dish. The surface of the absorber was coated with Pyromark 2000 flat black paint, which provided a measured solar-spectrum absorptivity of 96.5%. AEETES (Hogan, 1994) thermal modeling of the receiver on the TBC indicates thermal losses of 4.7kW_t or a receiver efficiency of about 93%. This analysis compares well with previous calorimetry testing on a similar second-generation receiver. CIRCE2 (Romero, 1994) modeling of the TBC predicts a peak flux on the receiver of approximately 70 W/cm² at 1000W/m² insolation.

Test Results

We performed the initial tests of the heat-pipe system with an open (380mm diameter) aperture in order to observe the absorber surface temperatures with a solar-blind infrared camera, which monitored the heat pipe operation. Several hot spots were detected near the top of the receiver, and we controlled these by masking the mirrors illuminating these parts of the dome. We limited the masking to 28 mirrors in order to match the input conditions of the DIR testing. The hotspots were controlled with these masks, all located on the bottom 4 rows of mirrors. We added the 220 mm aperture for performance testing.

The system was tested for approximately ½ hour, with the Direct Normal Insolation steady at about 1070 W/m². The heat pipe control temperature was set to 800°C, which was the highest available setting in the engine control unit. At this temperature, the helium cycle temperature measured at the hot duct was 680°C. The peak temperature on the front of the absorber dome was approximately 830°C, as determined by thermal modeling and verified with the IR camera. Figure 7 shows the history of this particular test. At 11:44, the test was temporarily suspended by an incorrect tripout setting on the IR camera. At 11:56, the test was again interrupted by a failed thermocouple. Finally, at 12:02, we observed a bright area on the visual camera and stopped to

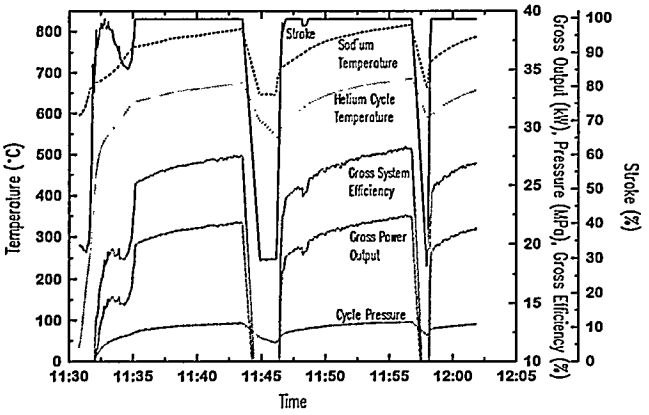

FIGURE 7. HEAT PIPE SYSTEM DATA DURING THE FINAL TEST WITH THE APERTURE INSTALLED.

investigate. This area proved to be a new hotspot, later confirmed with an added thermocouple, which terminated all testing.

Although the short run and low control temperature prevented the heat pipe system from reaching a steady state, some efficiency results were recorded. The maximum net power generated by the PCS was 21.4kW$_e$ at about 11:56. Adding the PCS parasitics of 945W, the gross power generated was 22.3kW$_e$. The solar power incident on the active area of the dish was 79.3kW$_t$, resulting in a gross efficiency of 28.1% sunlight to grid power. The PCS efficiency can be estimated by assuming the dish efficiency matches earlier receiver testing. The uncertainty of the dish efficiency is increased slightly because we did not clean the dish prior to this test. We estimated, based on prior calorimetry testing (Rawlinson, et al, 1990), that the dirty dish cost 2kW$_t$, resulting in 69.8kW$_t$ to the receiver at 1070W/m^2. The PCS efficiency is then 32% gross and 30.6% net. Assuming receiver thermal losses at 5kW$_t$ (The AEETES code predictions noted above neglect some conductive thermal losses), the engine/alternator gross efficiency is 34.5%, or about 36.9% shaft efficiency. The system gross efficiency is not corrected for the dirty dish.

DISCUSSION

While the database of DIR testing is extensive, the results for the heat pipe testing were limited by the receiver difficulties, and need to be repeated at a later date. The heat pipe testing duration was insufficient to reach steady state. However, some comparisons can be made from this preliminary data.

In order to properly compare the data, some of the operating conditions must be normalized. The engine performance is strongly dependent on the hot and cold temperatures (Carnot), the cycle pressure, and the stroke. STM typically collapses their performance data by plotting the power output vs. (1-Tau) where Tau is the water outlet temperature divided by the average cycle temperature. However, this requires consistent pressure and stroke settings, which is not easy during the on-sun tests. Through data comparison, we developed a factor that generally collapses the data to a straight line:

$$(1-T_{cwo}/T_{cyc})(P_{cyc}/P_o*\text{Stroke}/100)^{0.5}$$

where:

T_{cwo}= Cooling water outlet temperature (°K)
T_{cyc}= Average cycle temperature (°K)
P_{cyc}= Cycle pressure (Mpa)
P_o= Design cycle pressure, =13Mpa
Stroke is in percent of full stroke

The data plotted with this technique collapses to a straight line except during shutdown transients, where the hot duct thermocouple lags behind the actual hot-duct temperature. During startup transients, the engine controller slowly ramps up the setpoint temperature at a rate slower than the instrumentation thermal lag. The data was also limited to strokes greater than 50% and cycle pressures greater than 10MPa to avoid non-linear effects. Figure 8 displays the resulting collapsed data from performance mapping of the Helium and Hydrogen DIR systems as well as the one test of the heat pipe system. Since the x-axis factor includes the cycle temperature but not the heater head temperature, this plot shows the effect of the different systems on engine performance, but not system performance. Note that the hydrogen DIR and Helium Heat Pipe tests both demonstrate similar engine performance improvements over the Helium DIR test, amounting to about 2.5kW$_e$ improvement at similar internal engine conditions. Stine (1994) proposes a method of collapsing data from dish-Stirling systems that compares the power generated to the normal insolation, correcting for mirror cleanliness and cooling water temperature. However, this approach required more data than we had available from these tests, and so was not used.

During the DIR tests, 28 mirrors were covered to reduce the peak fluxes on the heater tubes to acceptable levels. Higher peak fluxes result in higher tube surface temperatures. The control system limited the temperature on the rear side of the tube (shaded from direct flux) to 800°C, which results in a front temperature in the peak flux of no more than STM's specified limit of 900°C. Thus, the power throughput of the DIR systems was limited by heater tube materials considerations. The phase

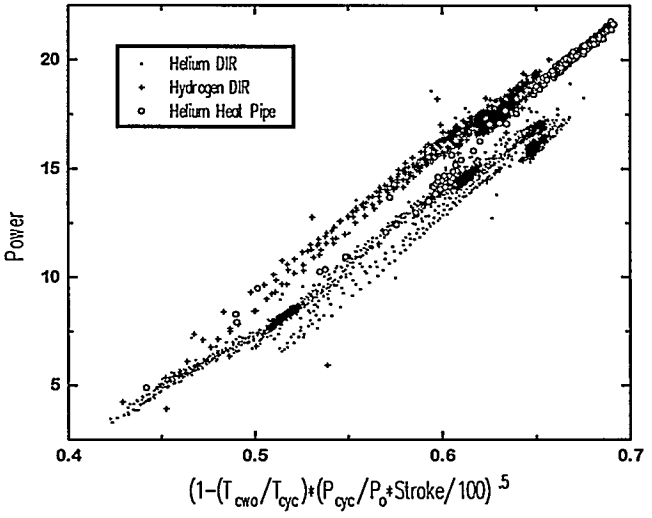

FIGURE 8. DATA FROM ALL THREE SYSTEMS COLLAPSED BY THE NORMALIZING FACTOR.

change in the heat pipe system accommodated the peak fluxes without significantly increasing the heat pipe surface temperatures. The vapor space was 800°C, which results in a peak absorber surface temperature of about 830°C and a heater head temperature of 800°C. The heat-pipe system performance was limited by the available power, rather than a materials limit. Even so, the heat pipe system generated 5kW$_e$ more than the DIR helium system (3kW$_e$ more than the hydrogen system). The improvements were realized through the improved engine efficiency as well as improved receiver efficiency. The heat pipe efficiency is about 93%, whereas the DIR receiver efficiency is about 85%.

During this heat pipe test, several hotspots appeared on the receiver. These hotspots were similar to those seen on a previous second-generation heat pipe. They are likely caused by poor wick bonding and oxide contamination of the wick. Further improvements in the receiver design and manufacturing processes should eliminate these difficulties on the next generation of felt-wick receivers. When these are eliminated, the mirror masks can be removed, resulting in more power available to the engine, and greater efficiency and power. Since the engine is already at full stroke, the temperature will rise to accommodate the increased input power. During this test, the peak receiver temperature was 70°C below that of the DIR, while more power was generated. Other heat pipe technologies are available now, such as sintered powder wicks, that already operate well at these power levels. We are pursuing the felt-metal wick aggressively because it has promise for significantly better operating margins than current technologies (Andraka, et al, 1995)

CONCLUSIONS

This series of tests presented a unique opportunity to compare the performance of a Stirling engine and a dish-Stirling system operated with a DIR receiver and separately with a heat pipe receiver. The heat pipe receiver improved the engine performance, the system efficiency, and the power capability of the dish-Stirling system over that of the DIR system under similar conditions.

The heat pipe receiver system improved the gross system efficiency from 23.2% on the helium DIR (25.6% hydrogen) to 28.1%, because both the receiver and engine efficiencies improved. The heat pipe receiver provided a slight improvement in engine performance over the DIR, roughly equivalent to that provided by a hydrogen working fluid in a DIR system. Under similar input power conditions, the heat pipe receiver generated 5kW$_e$ more than the helium DIR and 3kW$_e$ more than the hydrogen DIR. The improvements are primarily attributed to the decreased dead volume, uniform-temperature heat addition, and improved receiver efficiency. In addition, the peak system temperature in the heat pipe system was 70°C cooler for the same engine cycle temperatures. Thus, the heat pipe system will be able to accept more concentrated solar power, and generate more electrical power than the DIR under similar limiting conditions.

Further improvements are needed on the felt-wick heat pipe to realize the full benefits of this technology. The heat pipe system must be operated for significantly longer periods to generate the data for a thorough comparison and evaluation. Sufficient improvements are expected in the next year. In addition, further improvements should be realized by combining the heat pipe with the hydrogen-working-fluid engine. This is not currently possible because of the hydrogen permeation rates through the heater head materials. Advanced materials work in progress may reduce the permeation to acceptable levels.

REFERENCES

Adkins, D.R., Andraka, C.E., Bradshaw, R.W., Goods, S.H., Moreno, J.B., and Moss, T.A., 1996, "Mass Transport, Corrosion, Plugging, and Their Reduction in Solar Dish/Stirling Heat Pipe Receivers," *Proceedings of the 31st IECEC*, Washington DC.

Adkins, D.R., Moss, T.A., and Andraka, C.E., 1995, "An Examination of Metal Felt Wicks for Heat Pipe Applications," *Proceedings of the 4th ASME/JSME Solar Engineering Joint Conf.*, Lahaina, Maui, Hawaii.

Andraka, C.E., Adkins, D.R. Moss, T.A., Cole, H.M., Andreas, N.H., 1995, "Felt-Metal-Wick Heat-Pipe Solar Receiver," *Proceedings of the 4th ASME/JSME Solar Engineering Joint Conf.*, Lahaina, Maui, Hawaii.

Coleman, G.C. and Raetz, J.E., 1986, "Field Performance of Dish Stirling Solar Electric Systems," Paper No. 869136, *Proceedings of the 21st IECEC*, San Diego, CA.

Diver, R.B., Andraka, C.E., Moreno, J.B., Adkins, D.R., and Moss, T.A., 1990, "Trends in Dish Stirling Solar Receiver Design," Paper No. 905303, *Proceedings of the 25th IECEC*, Reno NV.

Hogan, R.E., 1994, "AEETES – A Solar Reflux Receiver Thermal Performance Numerical Model," *Journal of Solar Energy*, vol 52, number 2, pp167-178.

Rawlinson, K. Scott, and Gallup, Donald R., 1995, "On-Sun Testing of the STM4-120 Stirling Power Conversion System", paper 95-258, *Proceedings of the 30th IECEC, Orlando FL.*

Rawlinson, K. Scott, and Dudley, Vern E., "Test Bed Concentrator #1 Calorimetry Results", SAND89-2840, Sandia National Laboratories, Albuquerque, NM, Feb 1990.

Romero, V.J., 1994, "CIRCE2/DEKGEN2: A Software Package for Facilitated Optical Analysis of 3-D Distributed Solar Energy Collectors," SAND91-2238, Sandia National Laboratories, Albuquerque, NM.

Stine, W.B., 1994, "Proposed Design Guidelines for Dish/Stirling Solar Electric Generating Systems," Paper No. AIAA-94-3943-CP, *Proceedings of the 29th IECEC*, Monterey, CA.

Washom, B., 1984, "Parabolic Dish Stirling Module Development and Test Results," Paper No. 849516, *Proceedings of the 19th IECEC*, San Francisco, CA.

This work was supported by the United States Department of Energy, under contract DE-AC04-94AL85000

DISCLAIMER